RSC Advances

PAPER

View Article Online
View Journal | View Issue

Cite this: *RSC Adv.*, 2020, **10**, 17673

Work function modification of PEDOT:PSS by mixing with barium acetylacetonate†

K. L. Woon, *[a] W. S. Wong,[a] N. Chanlek,[b] H. Nakajima,[b] S. Tunmee,[b] V. S. Lee,[c] A. Ariffin[c] and P. Songsiriritthigul[d]

Received 20th March 2020
Accepted 23rd April 2020

DOI: 10.1039/d0ra02575e

rsc.li/rsc-advances

Poly(3,4-ethylenedioxythiophene)polystyrene sulfonate (**PEDOT:PSS**) is often used as a hole injection and extractor for various organic electronic devices. This study investigated whether it is possible to n-dope **PEDOT:PSS** with barium acetylacetonate (**Ba(acac)$_2$**) to change its work function so that to be more suitable for electron injection and extraction. Molecular dynamics simulations suggested that barium cations can interact with the aromatic rings of PEDOT and the negatively charged sulfonate in PSS. At high doping concentration, we found that PEDOT became dedoped and precipitated resulting in a clear solution after filtration. The absence of the absorption peak of PEDOT at 263 nm indicates the removal of PEDOT after filtration. The shift in O 1s to a lower binding energy as seen in X-ray photoelectron spectroscopy suggested that the polystyrene sulfonic acids are being ionized to form barium polystyrene sulfonate (Ba–PSS). By spin-coating the solution on top of indium tin oxide, the work function can be adjusted to as low as 3.6 eV. The ability of such a mixture to inject and extract electrons is demonstrated using 2,7-bis(diphenylphosphoryl)-9,9′-spirobifluorene as an electron transporting layer. We attributed the lowering of the work function as the result of the formation of an interfacial dipole as large as 1.37 eV at the ITO/Ba–PSS interface.

Introduction

Poly(3,4-ethylenedioxythiophene)polystyrene sulfonate (**PEDOT:PSS**) is a polymer ionomer widely used in various electronic devices such as organic light emitting diodes,[1,2] supercapacitors,[3] field effect transistors,[4] photovoltaic cells[5,6] and many more due to its superior electronic and ionic conductivities, stability and solution processability. **PEDOT:PSS** consists of the insulating negatively charged poly(styrenesulfonate) (PSS) counter-balanced by the positively charged poly(3,4-ethylenedioxythiophene) (PEDOT). The maximum oxidation of PEDOT is one charge per three monomer units, with the hole polaron delocalized over the three monomers forming a quinoid structure[7] counter-balanced by the electron located at the sulfonate side group. The weakly interacting ionomers result in an expanded coil conformation forming a colloidal dispersion in water.

In recent years, much effort has been concentrated in deepening the work function of the **PEDOT:PSS**. Several attempts have been carried out such as the use of metal oxide as dopants in **PEDOT:PSS**,[8] surface treatment with alkyl alcohol[9] and addition of Nafion[10,11] are found to deepen the work function up to 6 eV. Lowering the work function of **PEDOT:PSS** seems to be less successful. **PEDOT:PSS** modified with polyethylenimine can only reduce the work function to 4.0 eV.[12,13] Hence, efforts have been concentrated on solution processable sodium bicarbonate,[14] polymer zwitterion,[15] lithium phenolate complexes[16] and ruthenium acetylacetonate[17] which are deposited below the aluminum electrode. The increase in the electron injection ability is found to be the result of formation of interfacial dipole between the conductive electrode which lowers the vacuum level of the semiconducting layer.[18,19] Recent efforts such as the use of self-compensated multivalent anions electron donors[20] is promising as the effective work function of silver can be reduced to as low as 2.4 eV.

The objective of this research is to investigate the possibility of n-doping the **PEDOT:PSS** and to study the mechanism of such effect. This will enable the use of solution processable low work function cathode opening up the potential of fabricating organic electronic devices without the use of high vacuum system hence reducing the cost of production significantly. In this research, we mixed Clevios™ **PEDOT:PSS** Al4083 with barium acetylacetonate (**Ba(acac)$_2$**) in the hope of n-doping the **PEDOT:PSS**. We found that the work function can be reduced as

[a]*Low Dimensional Material Research Center, Department of Physics, University Malaya, 50603, Kuala Lumpur, Malaysia. E-mail: ph7klw76@um.edu.my*

[b]*Synchrotron Light Research Institute, Nakhon Ratchasima, 30000, Thailand*

[c]*Department of Chemistry, Faculty of Science, University Malaya, 50603, Kuala Lumpur, Malaysia*

[d]*Research Network NANOTECH-SUT on Advanced Nanomaterials and Characterization, School of Physics, Suranaree University of Technology, Nakhon Ratchasima, 30000, Thailand*

† Electronic supplementary information (ESI) available. See DOI: 10.1039/d0ra02575e

low as 3.6 eV. X-ray photoelectron spectroscopy (XPS) and molecular dynamics simulations suggested that the polystyrene sulfonic acids (PSSH) is being deprotonated lowering the binding energy of O 1s resulting in the formation of Ba–PSS. We attributed the lowering of work function as a result of formation of interfacial dipole by Ba–PSS.

Methodology

Materials

Fig. 1 shows the chemical structure of the materials used. **PEDOT:PSS** solution (Clevios™ PVP AI4083) was purchased from Heraeus. 2,7-Bis(diphenylphosphoryl)-9,9′-spirobifluorene (**SPPO13**) was purchased from Luminescence Technology (Taiwan). **Ba(acac)$_2$** and 2,2,3,3-tetrafluoro-1-propanol 98% were bought from Sigma-Aldrich. All materials were purchased and used as received without further purification.

Device fabrications

Different blending ratios of **PEDOT:PSS** : **Ba(acac)$_2$** (1 : *X*) with *X* = 0.2, 0.5, 1 and 5 were prepared by adding 3 mg, 7.5 mg, 15 mg and 75 mg of **Ba(acac)$_2$** to 1 g of **PEDOT:PSS** solution respectively. Pristine **Ba(acac)$_2$** solution was prepared by adding 15 mg of **Ba(acac)$_2$** to 1 g of deionized water. **SPPO13** solution was prepared by dissolving 25 mg of **SPPO13** to 1 ml of 2,2,3,3-tetrafluoro-1-propanol. All the solutions were filtered by 0.45 μm poly(tetrafluoroethylene) filters before use unless otherwise stated. Electron only device has a device structure of ITO/**PEDOT:PSS** : **Ba(acac)$_2$** (1 : *X*)/**SPPO13** (100 nm)/CsF (1 nm)/Al (100 nm). All the Indium Tin Oxide (ITO) coated glass substrates were ultrasonically cleaned using deionized (DI) water, acetone, isopropyl alcohol and DI water again for 10 min, followed by oxygen plasma treatment for 5 min. Pristine **PEDOT:PSS** was spin-coated on pre-patterned ITO with spin speed of 500 rpm, 1000 rpm, 1500 rpm and 2000 rpm each 10 s. **PEDOT:PSS** : **Ba(acac)$_2$** (1 : *X*) samples were prepared by firstly spin coating **PEDOT:PSS** as buffer layer with similar recipe as pristine, before dispensing **PEDOT:PSS** : **Ba(acac)$_2$** (1 : X) solutions on top of first layer at 30 s at 2000 rpm. The fabricated devices were then annealed in glovebox with 120 °C for 10 min. For electron transporting device, the **SPPO13** solution was subsequently spin-coated on top of **PEDOT:PSS** : **Ba(acac)$_2$** (1 : *X*) and annealed with 100 °C for 15 min. Finally, CsF (1 nm) and Al (100 nm) were thermally evaporated through shadow mask at base pressure of 4.2×10^{-4} Pa. The current density (*J*), voltage (*V*) of the devices were characterized with Keithley 2612B System Sourcemeter. The thickness of all solution-processed films was measured using a profilometer (P-6 KLA-Tencor).

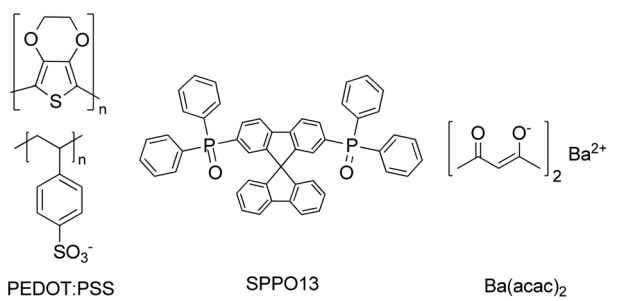

Fig. 1 Chemical structure of PEDOT:PSS, SPPO13 and Ba(acac)$_2$.

Characterizations

The work functions of the **PEDOT:PSS** : **Ba(acac)$_2$** (1 : *X*) were probed using ultraviolet photoelectron spectroscopy (UPS) at the soft X-ray undulator beamline BL3.2Ua in the Synchrotron Light Research Institute (SLRI) in Thailand. The samples were measured in a vacuum chamber under the base pressure of 1×10^{-9} mbar, and subject to UV radiation with a photon energy of 39.5 eV and a pass energy of 81.9 eV. The chemical compositions of the spin-coated films were investigated using the PHI5000 Versa Probe II X-ray photoelectron spectroscopy (XPS) system at the SUT-NANOTEC-SLRI joint research facility at SLRI in Thailand. The XPS spectra were collected using Al Kα (1486.6 eV) radiation, under the base pressure of 1×10^{-9} mbar. The surface morphology of the spin-coated films was measured using atomic force microscopy (AFM NT-MDT NTEG RA-Prima) operating at tapping mode. A PerkinElmer Lambda 750 UV-Vis-NIR was used to measure the material absorbance of the drop-casted and spin-coated **PEDOT:PSS** : **Ba(acac)$_2$** (1 : *X*) and **Ba(acac)$_2$** thin films on quartz substrates. The pH of the **PEDOT:PSS** : **Ba(acac)$_2$** (1 : *X*) solution was measured using Mettler Toledo™ FiveEasy™ F20 pH mV^{-1} under atmospheric pressure and ambient temperature. Calibration was performed with buffer solution of pH 4.01, pH 7 and pH 9.21 before pH measurement.

Computational calculations

For molecular dynamics simulations, the initial structures of PEDOT and PSS consisting five 3,4-ethylenedioxythiophene units and five styrene units respectively were minimized under semiempirical AM1 method to get the appropriate charge before subjecting for the molecular dynamics simulations for **PEDOT:PSS**. Four of each PEDOT and PSS were randomly distributed in the $100 \times 100 \times 100$ Å^3 box and sampled at 300 K under NVT periodic boundary condition for 500 ps with the time step of 1 fs using CHARMM force field in HyperChem package. Geometry optimizations were calculated using density functional theory (DFT) as implemented in the Terachem 1.9 software using unrestricted wB97XD functional at def2SVP basis level.[21] The calculations were performed using a GPU server that had 64 GB RAM installed to support eight Tesla K10 graphic cards. Milliken charge obtained from optimized structure of **Ba(acac)$_2$** at wB97XD functional using def2-QZVP basis is used for molecular dynamics simulations. 10 of such molecules were added randomly in the system to be run for another 500 ps. The final structures were minimized using the steepest descent method until the convergence of 0.1 kcal (Å mol)$^{-1}$ was obtained. Structural dynamics, potential energy, interaction energy between PEDOT and PSS of the systems with/without **Ba(acac)$_2$** were compared and analyzed.

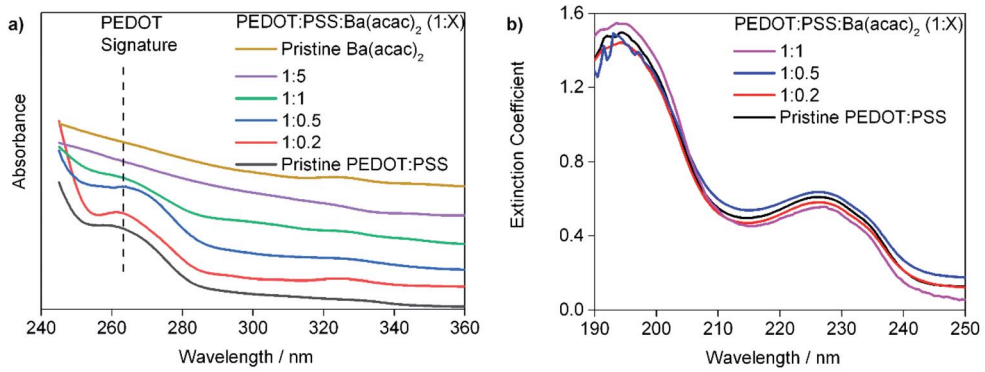

Fig. 2 The ultraviolet absorption spectroscopic data of (a) drop-casted films (b) films formed from spin-coated filtered solution.

Results and discussion

When we mixed **Ba(acac)$_2$** into **PEDOT:PSS**, we observed a certain degree of precipitation. The pH of **PEDOT:PSS** is 2.15, while the pH of the resulting solutions of **PEDOT:PSS** to **Ba(acac)$_2$** ratios for 1 : 0.2 and 1 : 0.5 are 2.24 and 2.45 respectively. At higher concentration, the pH becomes 5.42 and 8.13 for 1 : 1 and 1 : 5 ratios respectively. The change of pH indicates that chemical reactions must have taken place between **Ba(acac)$_2$** and **PEDOT:PSS**. We noticed that filtered mixtures at the ratios of 1 : 1 and 1 : 5 solutions are clear. The **Ba(acac)$_2$** solution (15 mg ml^{-1}) has a pH 7.11. Fig. 2(a) and (b) show the ultraviolet absorption spectroscopic data of drop-casted and spin-coated filtered solutions respectively. The drop-casted films are used since the absorbance of PEDOT in the UV is very weak. The absorbance in Fig. 2(a) was vertically translated to provide better clarity of the peak at 265 nm. We can see that the absorbance peak at 265 nm (which is very weak if the thickness of the film is too thin) decreases with increasing concentration of **Ba(acac)$_2$** as seen in Fig. 2(a). The absorbance

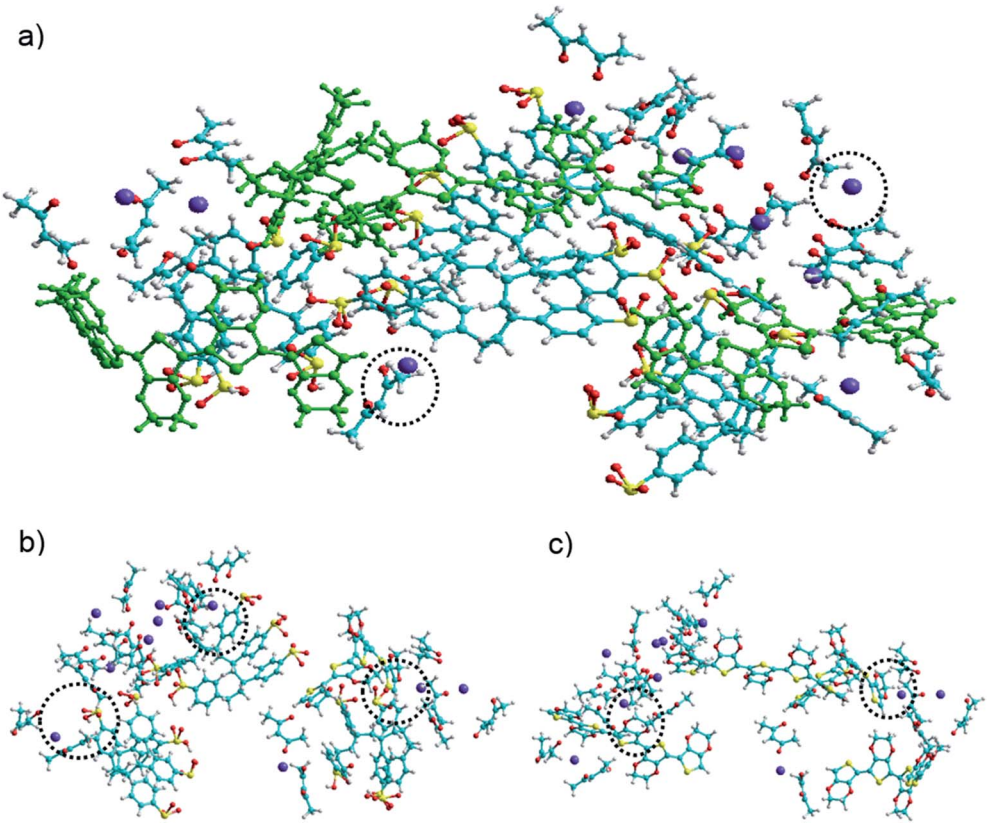

Fig. 3 (a) Equilibrium structure of assembly of **PEDOT:PSS** and **Ba(acac)$_2$** without water at 300 K. The highlight (dot circles) are the **Ba(acac)$_2$** and the green color are the PEDOT units. (b) Interaction between sulfonate and Ba^{2+}. (c) Interaction between aromatic bonds and Ba^{2+} from dissociated **Ba(acac)$_2$** as highlighted in dot circles.

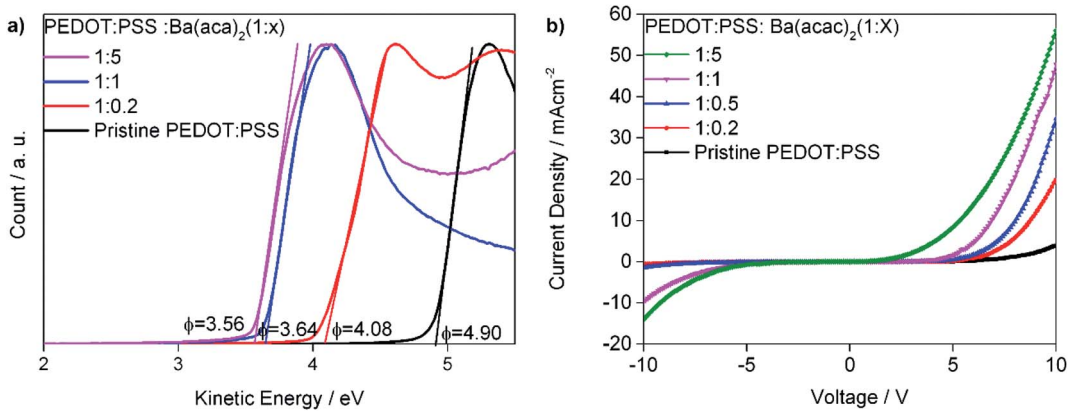

Fig. 4 (a) Work function of **PEDOT:PSS** with different concentrations of **Ba(acac)$_2$**. (b) The current–voltage behavior of device structure of ITO/**PEDOT:PSS** : **Ba(acac)$_2$**/**SPPO13**/CsF/Al.

peak at 265 nm corresponds to the aromatic transition of single ethylenedioxythiophene monomer in PEDOT.[22] Fig. 2(b) shows the extinction coefficient as defined in complex refractive index of the spin-coated films. The peaks at 195 nm and 225 nm correspond to transitions from the PSS aromatic rings[23,24] remain clearly seen. In order to gain insights on how **Ba(acac)$_2$** and **PEDOT:PSS** interact, molecular dynamics simulations are carried out.

Fig. 3(a) shows the assembly of **PEDOT:PSS** : **Ba(acac)$_2$** without water with dot circle highlighting the **Ba(acac)$_2$** molecules remained intact. However, some **Ba(acac)$_2$** molecules have disassociated as seen in the molecular dynamics simulations. Careful inspection of the assembly of the molecules, we can identify two types of interactions: coulombic attractions between Ba^{2+} and the sulfonate of PSS as seen in Fig. 3(b) and cation–π interactions between Ba^{2+} with aromatic π fragments in PEDOT as depicted in Fig. 3(c). Based on CHARMM force field, the interaction energy between PEDOT and PSS is 80.3 kcal mol^{-1} while its interaction with **Ba(acac)$_2$** is 115 kcal mol^{-1}. The higher interaction energy in the presence of **Ba(acac)$_2$** indicated interaction between PEDOT and PSS is weakened. In water, the poly(styrenesulfonate) acid (PSSH) can exist in equilibrium between PSS^- and H^+. We expect that as more Ba^{2+} are bound to sulfonate, more PSSH dissociates into PSS^- and H^+ ions in order to maintain the equilibrium while excess H^+ ions recombine with acetylacetonate ions to form acetylacetone until all poly(styrenesulfonate) acids are being deprotonated. This could explain why the acidity of **PEDOT:PSS** is being reduced.

Since precipitates can be detrimental to devices, we filtered the solutions just before spin-coating. Fig. 4(a) shows the work functions of **PEDOT:PSS** with different concentrations of **Ba(acac)$_2$**. The **PEDOT:PSS** has a work function of 4.90 eV for Clevios P VP Al4083. Increasing the amount of **Ba(acac)$_2$** into **PEDOT:PSS** lowers the work functions to 4.08 eV, 3.64 eV and 3.56 eV for the ratios of 1 : 0.2, 1 : 1 and 1 : 5 respectively. 1 : 0.5 are not shown since the work function is very similar to 1 : 0.2. Note that, **Ba(acac)$_2$** on top of the ITO has a work function of 4.06 eV while the 1 : 1 and 1 : 5 ratios have lower work functions than **Ba(acac)$_2$**. Fig. 4(b) shows the current–voltage behavior of electron transporting **SPPO13** with a device structure of ITO/**PEDOT:PSS** : **Ba(acac)$_2$**/**SPPO13**/CsF/Al. CsF/Al is an excellent injection layer and electrons are expected to be injected with ease from the CsF/Al.[25,26] As pristine **PEDOT:PSS** is not a perfect electron blocker, injected electron can be recombined in the hole polaron of PEDOT giving rise to current at high forward

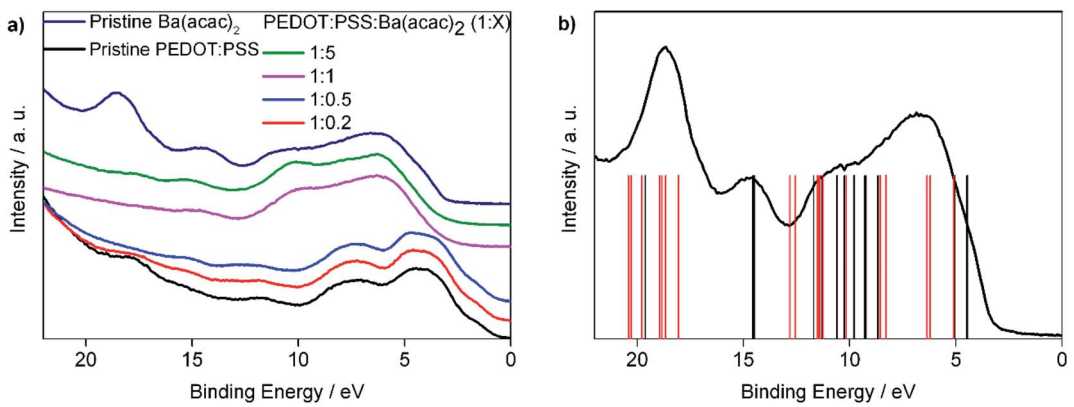

Fig. 5 (a) UPS spectra of **PEDOT:PSS** with different concentrations of **Ba(acac)$_2$** (b) the energy levels of **Ba(acac)$_2$** with the red vertical bars correspond to excitation of the whole molecules while the black vertical bars correspond to the counter ions only overlapping with UPS spectra.

bias voltage *i.e.* ~3 mA cm^{-2} at 10 V. However, at reverse bias, little current is detected implying that **PEDOT:PSS** is a poor electron injector as expected. In short, the forward bias indicates the ability for the interface to extract electrons while the reverse-bias indicates its ability to inject electrons. Addition of **Ba(acac)$_2$** drastically enhances such behavior in particular at a higher concentration of **Ba(acac)$_2$**. The lowest unoccupied molecular orbital (LUMO) of **SPPO13** is 2.91 eV and the interfacial dipole between **PEDOT:PSS : Ba(acac)$_2$** at 1 : 1 ratio is negligible as seen in Fig. S1.† This indicates an electron injection barrier of 0.6–0.7 eV even at high concentration of **Ba(acac)$_2$**. For the ratio of 1 : 1, the forward bias electron current density is very similar to the electron only device published elsewhere.[27]

We noticed that UPS spectra can be approximately divided into two groups as shown in Fig. 5(a). We shifted the UPS spectra so that the first peak of each curve coincided with the rest of the other samples. For the ratios at 1 : 0.2 and 1 : 0.5, the low energy UPS spectra are very similar to the pristine **PEDOT:PSS** while at higher ratios (1 : 1 and 1 : 5) the differences are obvious compared with pristine **Ba(acac)$_2$**. This is in agreement so the fact that the 1 : 1 and 1 : 5 filtered solutions are clear while the 1 : 0.2 and 1 : 0.5 are not. However, 1 : 1 and 1 : 5 are not **Ba(acac)$_2$** solutions, in particular the peak at 18.6 eV for **Ba(acac)$_2$** is absent in all other ratios. The energy levels are obtained from the DFT optimized **Ba(acac)$_2$** structure and these energies are compared with the UPS spectra which are subtracted from the secondary electron background as shown in Fig. 5(b). The red vertical bars correspond to excitation of electron clouds involving both barium and acetylacetonate ions. It is clear that the peak at 18.6 eV composed mainly from the excitations that involve the barium ions with the list of electronic orbitals can be found at Fig. S2.† This indicates that **Ba(acac)$_2$** is likely to have been disassociated which is consistent with the molecular dynamics simulations. The reduction of acidity of **PEDOT:PSS** resulted in the dedoping of **PEDOT:PSS**. In previous studies, mixing sodium poly(styrene sulfonate) (Na–PSS) with barium chloride resulted in an exothermic reaction forming poly(styrene sulfonate) (Ba–PSS).[28] Here, we suspected that Ba–PSS might have formed. The dedoping of **PEDOT:PSS** can inevitably lead to the separation of PEDOT and PSS that could result in precipitation.

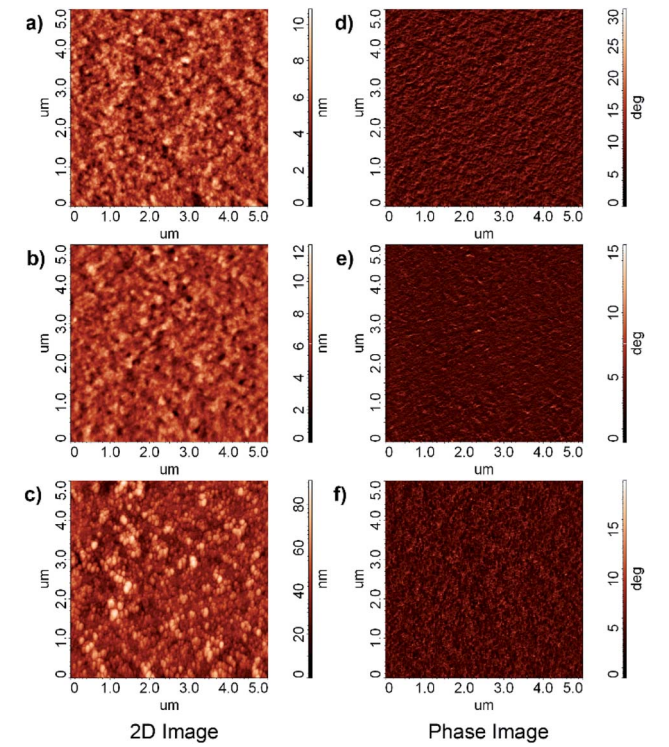

Fig. 6 Surface morphology for (a) PEDOT:PSS (b) PEDOT:PSS : Ba(acac)$_2$ at 1 : 0.2 (c) at 1 : 1 ratios. Phase image for (d) PEDOT:PSS (e) PEDOT:PSS : Ba(acac)$_2$ at 1 : 0.2 (f) at 1 : 1 ratios.

Fig. 6(a)–(c) are the surface morphology for **PEDOT:PSS : Ba(acac)$_2$** at different concentrations. The root means square roughness (R_a) are 1.35 nm, 1.29 nm and 10.9 nm for pristine **PEDOT:PSS**, 1 : 0.2 and 1 : 1 ratios respectively. It is clear that the morphology has changed from the fiber-like network structure at low concentration of **Ba(acac)$_2$** to compacted elongated sphere and pearl necklace-like appearance. The compactification could be due to the coulombic attraction between Ba^{2+} with the negatively charged sulfonate within the same chain or different chains that collapsed the chains (coil-globule transition).[29] In terms of phase image of **PEDOT:PSS**, the bright color is often referred to as PEDOT-rich domains while PSS-rich domains often appear darker (Fig. 6(d)).[30] When 20% loading is added into **PEDOT:PSS**, the surface becomes noticeably darker, possibly an indication of PSS enriched surface (Fig. 6(e)). Fig. 6(f) shows the morphology of **PEDOT:PSS : Ba(acac)$_2$** at 1 : 1 ratio with the uniform distributed fibrils nature as a background juxtaposed by the appearance of elongated sphere and pearl necklace-like states. The thickness of the resulting thin films are (84 ± 9) nm, (38 ± 3) nm, (43 ± 2) nm and (7 ± 1) nm for **PEDOT:PSS**, at ratios of 1 : 0.2, 1 : 0.5 and 1 : 1 respectively. For 1 : 5 ratio, the thickness of the film is too thin to be measured reliably. If a solution of 15 mg ml^{-1} **Ba(acac)$_2$** are spin-coated, we found the resulting thickness will be less than 5 nm (see Fig. S3†).

In order to elucidate the interactions between **PEDOT:PSS** and **Ba(acac)$_2$**, we carried out XPS measurements. Fig. 7(a) is the S 2p core level displaying two signature peaks. The higher binding energy (~168 eV) belongs to PSS because of the electronegative oxygen attached to the sulphur atoms in the sulfonate fragment of the PSS. The S 2p signature from PEDOT is far weaker with a composition ratio of ~ 1 : 8.9 (the ratio of PEDOT to PSS) indicating a richer PSS at the top surface in comparison with homogeneous mixed Al4083 which has a ratio of 1 : 7.5. At 20% loading, the ratio of PEDOT to PSS does not change while at 50% loading the ratio has changed to 1 : 11. At even higher loading of **Ba(acac)$_2$**, the S 2p peak for PEDOT has reduced significantly with high noise and hence reliable PEDOT to PSS ratio cannot be obtained (see Fig. S4†). The composition of the surface are measured at a ratio of sulphur S 2p to barium Ba 4p corrected by photoionization cross-section giving the elemental ratio of 25 : 1, 14 : 1, 2.6 : 1 and 1.8 : 1 for **PEDOT:PSS : Ba(acac)$_2$** at the ratios of 1 : 0.2 1 : 0.5, 1 : 1 and 1 : 5 respectively as seen in Fig. S5.† This might suggest that at

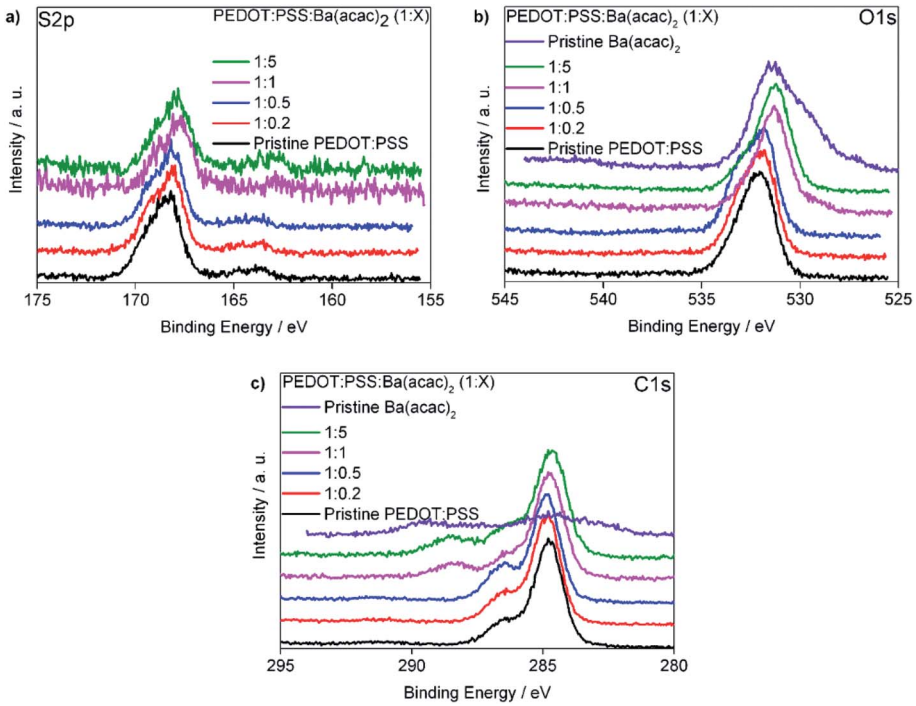

Fig. 7 XPS spectra for **PEDOT:PSS** : **Ba(aca)$_2$** at various concentrations (a) S 2p (b) O 1s (c) C 1s.

higher ratios Ba–PSS may have formed. Fig. 7(b) shows the binding energy of O 1s for the mixtures and the pristine **Ba(acac)$_2$**. The two peaks in **Ba(acac)$_2$** are contributed by the negatively charged O–C (lower binding energy at ~ 529.3 eV) and neutral O=C (~531.5 eV) in acetylacetonate ions. Usually metal acetylacetonates bind to metal through the central carbon atom in a coordination complex. However, our XPS suggested that the barium only bond through one oxygen-bonded acac ligand. The optimized structure obtained through uwB97X/def2SVP level and even at a higher basis level at def2QZVP confirmed this as seen in Fig. S6.† Attempts to create the initial complex by bonding through the central carbon-bonded acac ligand resulted in bad geometry upon optimization. We attributed the shift of the binding energy of O 1s to a lower binding energy due to the ionization of S(=O)$_2$–OH fragment from PSSH consistent with our understanding that Ba–PSS has formed. Fig. 7(c) shows the binding energy of C 1s for the mixture and the pristine **Ba(acac)$_2$**.The peak at 284.8 eV corresponds to the C atoms in the PSS and the C atoms in the PEDOT which are not bonded to the oxygen. The peak at a higher binding energy 286.5 eV corresponds to those C atoms in the PEDOT which are bonded to oxygen atoms. A new peak at 288.3 eV appeared at a higher concentration of **Ba(acac)$_2$**. We assigned this to the C=O bonds in the acetylacetone residuals that are still embedded inside the thin films. This peak is located very close to the peak at ~289 eV which we assigned to the C=O and C–O$^-$ of the acetylacetone in **Ba(acac)$_2$**. Since UPS spectra indicated that upon mixing of **Ba(acac)$_2$** and **PEDOT:PSS**, most Ba^{2+} cations dissociated from the acetylacetonate counter ions and since, acetylacetone is a volatile liquid with a boiling point of 140 °C, one would assume that any remaining acetylacetone will be evaporated in high vacuum (UPS and XPS chambers) and the residual of acetylacetone unlikely to remain yet the detection of its signature at XPS (288.3 eV) indicates not all **Ba(acac)$_2$** are dissociated consistent with the molecular dynamics simulations.

According to Stephan van Reenen *et al.* who studied the magnitude of the work functions modification by X^+PSS^- with X = H^+, Li^+ Na^+, a trend is observed in terms of ion size.[31] Caesium stearate, an ionic electrolyte with a very large counter ion has been shown to improve the electron injection of the aluminum.[32] Based on the trend of X^+PSS^-, Stephan van Reenen *et al.* suggested that the relatively large size of the Cs^+ ion might make image charge screening more favorable. Nevertheless, n-type doping by Cs^+ may also explain the observed results. The highest occupied molecular orbital (HOMO) and the lowest unoccupied molecular orbital (LUMO) of Ba–PSS are located at PSS and Ba respectively as shown in Fig. 8. It is important to note that the LUMO of Ba–PSS is 0.53 eV, a value greater than zero indicating that any added electrons are unbounded, ie the electrons are free to move. Motivated by this finding, we studied $Y^{2+}PSS^{2-}$ with Y = Be^{2+}, Mg^{2+}, Ca^{2+}, Sr^{2+} and Ba^{2+} and X^-PSS^+

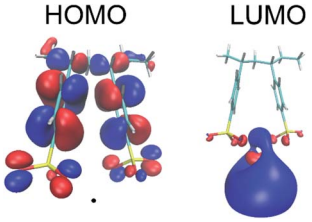

Fig. 8 The HOMO and LUMO of Ba–PSS.

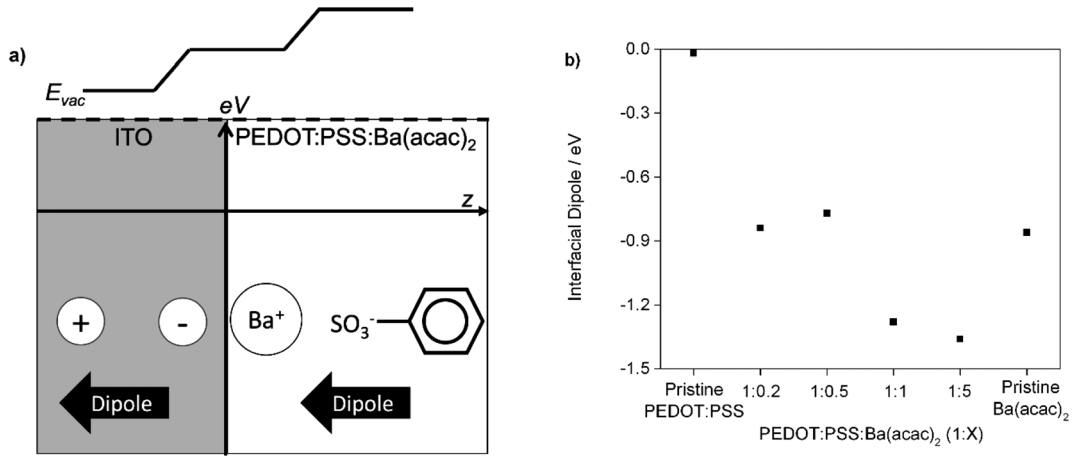

Fig. 9 (a) The mechanism of formation of interfacial dipole along with the image charge that moves the vacuum level upward (b) interfacial dipole for **PEDOT:PSS**, **Ba(acac)$_2$** and **PEDOT:PSS** : **Ba(acac)$_2$** at different ratios.

with X= Li^+, Na^+,K^+, Rb^+ and Cs^+ systems. We found that all the systems studied, the LUMO energies are always positive with the LUMOs are located at Ba^{2+}, Sr^{2+} and Cs^+ metal counter ions while for other alkali counter ions, the LUMOs are located at the PSS which can be seen in Fig. S7.†

We know that the wettability of the ITO surface is enhanced after oxygen plasma treatment. Because PSS has a flexible backbone and the Ba^{2+} cations have high degree of freedom in water solution compared with PSS, the Ba^{2+} cations can preferentially reorientate on the ITO surface during the film formation. The barium ions would polarize the ITO to form an electric field (image charges) that opposes the desorption of positive charged ions. Since the ITO is a highly doped n-type semiconductor, the static dielectric constant should be large enough to stabilize the image charges. The collective of positive charge and the negative charge of sulfonates create a dipole near the ITO surface. Since the dipole of the image charges is the same direction as the dipole of Ba–PSS, the total dipole is enhanced as shown in Fig. 9(a). Hence, we attributed the change of work function as a result of formation of interfacial dipole. This is particularly true at the ratios of 1 : 1 and 1 : 5. The vacuum levels between ITO and **PEDOT:PSS** : **Ba(acac)$_2$** at different ratios can be obtained by minus the high energy cut-off onset from the UPS spectra onset (Fig. S8†) from the photon energy (39.5 eV). The vacuum levels of ITO and **PEDOT:PSS** : **Ba(acac)$_2$** at different ratios are not aligned at same height indicated the presence of interfacial dipole. Fig. 9(b) shows the interfacial dipole formed by the various ratios of **PEDOT:PSS** : **Ba(acac)$_2$** on the ITO. The interfacial dipole at the ratios of 1 : 1 and 1 : 5 are 1.26 eV and 1.37 eV respectively indicating an upward vacuum shift that lowers the effective work function. This is larger than the vacuum shift of pristine **Ba(acac)$_2$** (~0.93 eV) possibly indicating the flexibility of counter ions might be important for reorientation. Since the thickness is less than 10 nm (1 : 1 and 1 : 5 ratios), the charge injection/extraction can be dominated by quantum tunneling. The vacuum shift for 1 : 0.2 and 1 : 0.5 ratios are ~0.85 eV and 0.77 eV respectively and the thickness of these films are larger than 10 nm. Electron conduction for thicker films can occur through combination of ionic motion, hopping through the barium ions within these layer under applied bias.[33]

Conclusions

We have demonstrated that by mixing high concentration of **Ba(acac)$_2$** into **PEDOT:PSS**, formation of PEDOT precipitates and Ba–PSS ionomer salts has occurred. At high concentration of **Ba(acac)$_2$**, more PSSH is being deprotonated as evident from the XPS. Filtering out the PEDOT precipitates before spin-coating lowered the work function of ITO to as low as 3.6 eV. We attributed the lowering of work function as a result of the formation of interfacial dipole from the reorientation of Ba cations on top of the ITO surface. This finding implies that ionic polymer with barium or caesium as counter cation can be used to lower the effective work function of a surface. Since PSSH is an insulating polymer, we anticipate that future works will involve the use of highly conjugated polymer as an ionomer.

Conflicts of interest

There are no conflicts to declare.

Acknowledgements

This work was financially supported by University Malaya Postgraduate Research Grant (PG043-2015B), MyBrainScholarship and University Malaya Impact Orientated Interdisciplinary Research Grant (IIRG005A-19FNW). The Research Network NANOTEC program of the National Nanotechnology Center of Thailand is also acknowledged for partial financial support.

References

1 K. L. Woon, W. S. Wong, N. Chanlek, H. Nakajima, S. Tunmee, C. Songsiriritthigul, V. S. Lee and P. Songsiriritthigul, *Org. Electron.*, 2019, **74**, 1–6.

2 S. Chen, Q. Zhang, W. Shang, L. Liu, H. Yu, S. Zhang, L. Deng, M. Wang, M. Wang, X. Li, B. Mi and W. Huang, *Sci. Rep.*, 2018, **8**, 8155.
3 Y. Liu, B. Weng, J. M. Razal, Q. Xu, C. Zhao, Y. Hou, S. Seyedin, R. Jalili, G. G. Wallace and J. Chen, *Sci. Rep.*, 2015, **5**, 17045.
4 S. H. Kim, J. Kim, S. Nam, H. S. Lee, S. W. Lee and J. Jang, *ACS Appl. Mater. Interfaces*, 2017, **9**, 12637–12646.
5 C. T. Howells, S. Saylan, H. Kim, K. Marbou, T. Aoyama, A. Nakao, M. Uchiyama, I. D. W. Samuel, D.-W. Kim, M. S. Dahlem and P. André, *J. Mater. Chem. A*, 2018, **6**, 16012–16028.
6 T. J. Whitcher, N. A. Talik, K. Woon, N. Chanlek, H. Nakajima, T. Saisopa and P. Songsiriritthigul, *J. Phys. D: Appl. Phys.*, 2014, **47**, 055109.
7 D. Kim and I. Zozoulenko, *J. Phys. Chem. B*, 2019, **123**, 5160–5167.
8 A. Kanwat and J. Jang, *RSC Adv.*, 2016, **6**, 114800–114807.
9 M. R. Lenze, N. M. Kronenberg, F. Würthner and K. Meerholz, *Org. Electron.*, 2015, **21**, 171–176.
10 S. A. Mauger, J. Li, Ö. T. Özmen, A. Y. Yang, S. Friedrich, M. D. Rail, L. A. Berben and A. J. Moulé, *J. Mater. Chem. C*, 2014, **2**, 115–123.
11 K. H. Yeoh, N. A. Talik, T. J. Whitcher, C. Y. B. Ng and K. L. Woon, *J. Phys. D: Appl. Phys.*, 2014, **47**, 205103.
12 Z. Li, F. Qin, T. Liu, R. Ge, W. Meng, J. Tong, S. Xiong and Y. Zhou, *Org. Electron.*, 2015, **21**, 144–148.
13 Y. Zhang, L. Chen, X. Hu, L. Zhang and Y. Chen, *Sci. Rep.*, 2015, **5**, 12839.
14 D. X. Long and Y.-Y. Noh, *J. Mater. Chem. C*, 2018, **6**, 12871–12878.
15 M. Ruscello, S. Stolz, D. L. Gonzalez Arellano, F. Ullrich, S. Hillebrandt, E. Mankel, A. Pucci, W. Kowalsky, T. Emrick, A. L. Briseno and G. Hernandez-Sosa, *Org. Electron.*, 2017, **50**, 384–388.
16 Z. Q. Zhao, S. You, J. Huang, L. Yuan, Z. Y. Xiao, Y. Cao, N. Cheng, L. Hu, J. F. Liu and B. H. Yu, *J. Mater. Chem. C*, 2019, **7**, 9735–9742.
17 W. Chen, S. Luo, Z. Wan, X. Feng, X. Liu and Z. He, *Opt. Express*, 2017, **25**, A253–A263.
18 C.-H. Wu, K.-W. Tsai, W.-J. Huang, C.-Y. Wu, T.-Y. Chen, T.-F. Guo, Y.-J. Hsu and T.-C. Wen, *Adv. Mater. Interfaces*, 2016, **3**, 1500621.
19 W. Liu, T. Liang, Q. Chen, Z. Yu, Y. Zhang, Y. Liu, W. Fu, F. Tang, L. Chen and H. Chen, *ACS Appl. Mater. Interfaces*, 2016, **8**, 9254–9261.
20 C. G. Tang, M. N. Syafiqah, Q.-M. Koh, C. Zhao, J. Zaini, Q.-J. Seah, M. J. Cass, M. J. Humphries, I. Grizzi, J. H. Burroughes, R.-Q. Png, L.-L. Chua and P. K. H. Ho, *Nature*, 2019, **573**, 519–525.
21 T. Lu and F. Chen, *J. Comput. Chem.*, 2012, **33**, 580–592.
22 A. Elshchner, S. Kirchmeyer, W. Lovenich, U. Merker and K. Reuter, *PEDOT. Principles And Applications Of An Intrinsically Conductive Polymer*, 2011.
23 Y. H. Kim, C. Sachse, M. L. Machala, C. May, L. Müller-Meskamp and K. Leo, *Adv. Funct. Mater.*, 2011, **21**, 1076–1081.
24 Y. Xia, K. Sun and J. Ouyang, *Energy Environ. Sci.*, 2012, **5**, 5325–5332.
25 H.-X. Wei, Q.-D. Ou, Z. Zhang, J. Li, Y.-Q. Li, S.-T. Lee and J.-X. Tang, *Org. Electron.*, 2013, **14**, 839–844.
26 R. Zheng, W. Huang, W. Xu and Y. Cao, *Synth. Met.*, 2012, **162**, 1919–1922.
27 S. O. Jeon, K. S. Yook, C. W. Joo and J. Y. Lee, *J. Mater. Chem.*, 2009, **19**, 5940–5944.
28 M. Hansch, H. P. Kaub, S. Deck, N. Carl and K. Huber, *J. Chem. Phys.*, 2018, **148**, 114906.
29 M. Hansch, B. Hämisch, R. Schweins, S. Prévost and K. Huber, *J. Chem. Phys.*, 2018, **148**, 014901.
30 B. Lu, H. Yuk, S. Lin, N. Jian, K. Qu, J. Xu and X. Zhao, *Nat. Commun.*, 2019, **10**, 1043.
31 S. van Reenen, S. Kouijzer, R. A. J. Janssen, M. M. Wienk and M. Kemerink, *Adv. Mater. Interfaces*, 2014, **1**, 1400189.
32 G. A. H. Wetzelaer, A. Najafi, R. J. P. Kist, M. Kuik and P. W. M. Blom, *Appl. Phys. Lett.*, 2013, **102**, 053301.
33 C.-C. Chueh, C.-Z. Li and A. K. Y. Jen, *Energy Environ. Sci.*, 2015, **8**, 1160–1189.

